International Journal of Heat and Technology
Vol. 42, No. 4, August, 2024, pp. 1434-1446
Journal homepage: http://iieta.org/journals/ijht

Investigation of Copper Backing Plate Effects in Stainless Steel Welding Distortion, Heat Distribution, and Residual Stress

Mohammed S. Mohammed[1*], Mohammed D. Hamdey[2], Ahmed Hashim Kareem[3], Hasan Shakir Majdi[4]

[1] Training and Workshop Center, University of Technology- Iraq, Baghdad 10066, Iraq
[2] Department of Mechanical Engineering, College of Engineering, Al-Nahrain University, Baghdad 64040, Iraq
[3] Mechanical Department of Amarah Technical Institute, Southern Technical University, Basra 62001, Iraq
[4] Department of Chemical Engineering and Petroleum Industries, Al-Mustaqbal University College, Hillah 51001, Iraq

Corresponding Author Email: mohammed.s.mohammed@uotechnology.edu.iq

https://doi.org/10.18280/ijht.420433

Received: 5 January 2024
Revised: 14 July 2024
Accepted: 30 July 2024
Available online: 31 August 2024

Keywords:
ANSYS simulation, deformation, thermal, mechanical analysis, SOLIDWORKS, copper backing plate

ABSTRACT

The current study uses a Finite Element (FE) Method to forecast residual stresses and deformation caused by the GTA welding process. The authors use a 5 mm thick stainless steel plate for the analysis. Residual stress and distortion predictions are made by successfully coupling thermal and mechanical studies. Mechanical and thermal analyses of moving heat source-exposed plates were conducted sequentially. Applications such as ANSYS and SOLIDWORKS are used to do the FE analysis. In transient thermal analysis, the arc's heat input has been modeled using a Gaussian distribution. Consideration of temperature-dependent physical and mechanical parameters is integral to the modeling process. The welding heat in stainless steel welding and how it behaves inside the joint has significant effects in determining the welding joint distortion, mechanical properties, and the weldments fit with the design criteria due to stainless steel thermal properties. Subsequent mechanical analysis is fed the transient thermal histories to the model. Analyzing mechanical systems involves using the big displacement hypothesis. How restrictions influence distortion and residual stresses is quantitatively investigated. The anticipated stresses and distortion values are presented and discussed for various scenarios. Welding distortion was minimized when a copper backing plate was used, as shown by a lower maximum deformation measured compared to situations without the plate. The backing plate reduced maximum stress values and lowered residual stresses. A backing plate also made the fusion zone smaller and the temperature drop from the peak welding temperature to room temperature steeper. According to the research, using a copper backing plate during stainless steel welding may significantly reduce deformation and residual stresses. The results could improve stainless steel welding by choosing the best materials for backing plates and improving welding. Investigation results and the mathematical models of welding simulation can significantly improve stainless steel deformation-reducing techniques in many applications and introduce particular techniques to predicate the impacts of backing plates in such welding processes as food, chemical, Pharmaceutical, Oil and Gas, and water treatment industries.

1. INTRODUCTION

Because of its increased susceptibility, welding austenitic stainless steel raises severe concerns about deformation. In industries like shipbuilding, where a lot of work goes into fixing deformations, this problem is a significant obstacle [1]. Excessive stress applied to the weld joint during welding may give rise to various types of deformities. These shape changes can be seen when something gets shorter and squeezed or with correct change. They also show in the changing direction of structures while holding view pressure firmly. In addition, the fast heating and cooling that happens when welding results in unused stresses. Then, they can make little stretchy changes with visible deformations [2]. Therefore, damage from welding can make design and technological engineers worry about getting things right, even in the area of putting things together. Old studies have shown that these fears can be found correctly by using back plates [3]. To fix these issues properly, it is essential to lessen the impact of welding heat distribution and lower places that get damaged. This part is also sometimes called a heat-affected zone (HAZ). Furthermore, changing how you weld to have perfect welding without bad joints would be best. This means changing things like how quickly you weld and the amount of power used for this task. In the case of welding-treated steel, reducing residual stress necessitates carefully selecting a suitable material for the backing plate [4]. Copper backing plates offer advantages in that they demonstrate less deformation than other metals, such as steel and aluminum. As the material cools and solidifies at room temperature, one method for estimating the thermal stresses consists of observing the change in volume within the weld zone. If the stresses arising from heat compression surpass the yield strength of the parent metal, limited plastic deformation occurs. This plastic deformation alters the structure of the component and results in a permanent reduction in size. There are six primary forms in which distortion can manifest, one of which is angular distortion. Angular distortion is the term used to describe the rotational movement of a structure around the welding line [5]. This sort of deformation arises in butt joint when transverse shrinkage uneven throughout thickness direction. Studies have shown a higher degree of elastic contraction on the upper than the lower part, resulting in angular distortion [6]. Figure 1 illustrates how the shrinkage pressure adjustments across the thickness of the welding joint. Bending distortion is the same as turning change but is different because it affects joints not sideways but straight up and down to their bottom. Rotational deformation is when something gets turned in the same area due to local heating and sliding [7]. Models from simulations have been helpful in real work situations for some industries using finite element models (FEM). This has helped us learn how different supports change the quality of connections in welds, bending, and remaining stresses [8]. Moreover, this study's practical and empirical model analysis highlights the impact of incorporating copper backing plates during stainless steel welding. In essence, comprehensive comprehension of the deformation issues in stainless steel welding is imperative to achieve superior-quality welded joints and diminishing residual stresses [9]. The study aims to explain the effects of copper backing on stainless steel welding and give scientific information and data to improve ways of using copper backing, which helps reduce distortion and extra stress. This will finally make stainless steel structures welded in a better way and answer the questions about the expected distortion and the welding joints fitting with the design requirements when no backing plate is used.

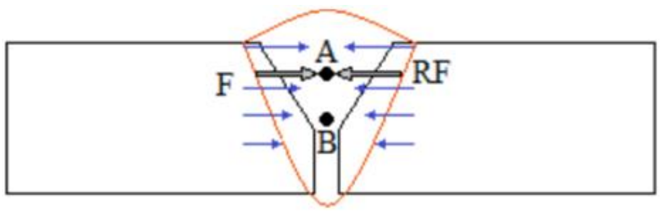

Figure 1. Angular distortion formation in single "V" groove butt welding. A: center of welded metal mass. B: center of transversal cross-section mass. F: The forces caused by the shrinkage in the transverse direction. RF: The resulting force caused by the shrinkage [10]

The Finite Element method simulates the parts' heat source and studies the past temperature influences, leftover stress, and total distortion [11, 12]. Imposing constraints during the finite element analysis is essential to reproduce residual stresses and deformations accurately. Some researchers have used single-point limits to predict residual stress in their studies. These constraints significantly affect the residual stresses generated in the components. Appropriate constraints are carefully selected to control lateral distortion in practical applications. Okano and Mochizuki [13] investigated the generation of precise deformations in thin metal plates using accurate measurements and computer models throughout the welding process. It was found that the buckling mode caused angular deformation in the lifestyles, which was established to be driven by utilizing longitudinal deflection. In addition, they conducted a thorough analysis of the influence of jig constraints using computer modeling. Suman and Biswas [14] and Zubairuddin et al. [15] found that preheating packages may reduce welding distortion in single-pass and multi-pass welding techniques. Duranton et al. [16] used 3D finite element models to quantify the deformation and residual stresses resulting from the multi-pass welding of 316 L stainless steel. Stamenković and Vasović [17] conducted a 3D finite element welding simulation to forecast residual stresses in the butt-welding of two carbon steel parts. Murugan et al. [18] examined residual stresses in AISI 304 stainless steel and V-groove low carbon steel with thicknesses of 6, 8, and 12 mm that were welded using the MMAW technique. The maximum residual stresses observed in low-carbon and stainless steel were 220 MPa and 193 MPa, respectively. These stresses were found in the center of the weld bead. The previous study investigated the influence of different pulsed gas tungsten arc (GTA) welding parameters on the residual stresses produced during the welding process. Zhu and Chao [19] investigated the behavior of 304 L stainless steel using friction stir welding to illustrate variations in transient temperature and residual stress. The investigation revealed a substantial reduction in longitudinal residual stress after the release of the fixture. The decrease in strength varied from 470 MPa to 60 MPa as the distance from the welding center increased. To evaluate residual stresses, Prasad and Sankaranarayanan [20] used adaptive grids dependent on temperature calculation. Meanwhile, Mollicone et al. [21] used many finite element models to investigate the effects of different modeling techniques on accurately simulating the thermo-elastic-plastic phases of the welding process. In addition, Cho et al. [22] used numerical analysis to ascertain the distribution of residual stress during welding and subsequent post-weld heat treatment in two multi-pass welds of thick plates.

Distortion and residual strains can lead to various complications in welded structures, ultimately leading to diminished performance. Residual stress distribution represents original stress present in welded construction and must considered in conjunction with impact of applied service loading. Although several experimental methods have been devised to quantify residual stress through destructive and non-destructive means, acquiring a comprehensive understanding of residual stress distribution is not feasible just through practical procedures. Therefore, computational simulation is crucial to solving these complex problems. Finite Element Method (FEM) software packages, such as ABAQUS, ANSYS, NASTRAN, and MARC, are commercially available and can be used to analyze welding thermal elastic-plastic stresses and distortion. The finite element analysis of welding involves the simulation of various phenomena, including temperature-dependent material behavior, non-linearity, the three-dimensional nature of the weld pool, welding processes, and phase transformation caused by changes in microstructure. Within the context of this research, ANSYS 2022R1 software was used to simulate the effects of copper backing plates on heat distribution, HAZ dimension, fusion zone width and penetration, deformation, and residual stresses in butt welding of stainless steel plates. The selection of stainless steel for the welding plates was based on its extensive use in manufacturing to fabricate structures and components, including bridges, steel structures, automotive parts, and industrial machine components. Numerical approaches have been employed to imitate several welding processes during the past two decades. Simulating a welding process digitally is quite intricate. The reason for this is that welding involves the application of high temperatures, material qualities dependent on temperature, and significant deformations. All the previous research in welding joint simulation was based on moving heat source extension in ANSYS software to simulate the welding line. Still, the problem with this technique was its limitations in accurate welding joint design simulation due to its dependence on straight line selection as a welding path. This study presents new techniques in welding joint design moving heat simulation by using the transit heat and static structure with a new approach of fusing joint design in SOLIDWORKS to simulate the arc moving with consideration of the joint design dimensions for more accurate results when exported to ANSYS for simulation purposes. This new technique solved the problem with the ready-moving heat source extension in ANSYS software, which didn't consider the high impacts of the welding joint design in welding heat generation, distribution, and its implications on deformation and residual stresses.

2. COMPUTATIONAL AND EXPERIMENTAL PROCEDURE

A welding simulation was performed according to the transient thermal ANSYS analysis. In this case, the welding method was assumed to be manual arc welding. Two models were created using SOLIDWORKS software according to the AWS (American Welding Society) single-V butt welding D1.6:2007 Structural Welding Code, as illustrated in Figure 2, to predict the impact of copper bucking plates on residual stresses and distortion of welded components. This standard requires only one pass with a 5/32-inch welding electrode to complete the joint and minimize the input heat.

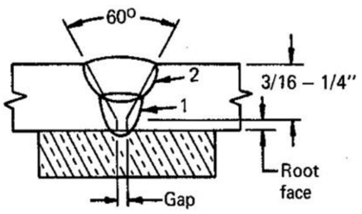

Figure 2. AWS standard joint design for 300 series with backing

The designed model's dimensions were 200 × 50 × 5 mm, with two models with and without backing, as shown in Figure 3(a) and Figure 3(b). Both models were exported to the ANSYS environment for FEM simulation. The two models meshed using ANSYS software, as shown in Figure 4(a) and Figure 4(b), and their mesh information is listed in Table 1. AISI 304 st. st material was used for the simulation, and its mechanical properties are listed in Table 2. The heat created by the arc of the electrode tip in ANSYS is simulated using a moving heat source extension. The heat source relocation or trip duration is simulated using the element birth and death approach. During element birth and death, the desired element is deactivated, resulting in its termination and rendering it unresponsive to any input. However, this is different during welding. The ANSYS program retains things labeled as "killed" and does not remove them. Instead, it makes them inert by progressively diminishing their stiffness with a substantial decrease coefficient. Nevertheless, the problem with these welding processes stems from their failure to consider the requirements for developing the welding connection. The welding simulation for a linear motion and unidirectional heat source may be promptly used in a simulation study. However, let us contemplate a situation where the heat source undergoes non-linear expansion or deviates from the ellipsoid Gaussian normal distribution. Hence, it is vital to devise and include a supplementary subroutine into ANSYS to accomplish the task of this thermal energy generator [10].

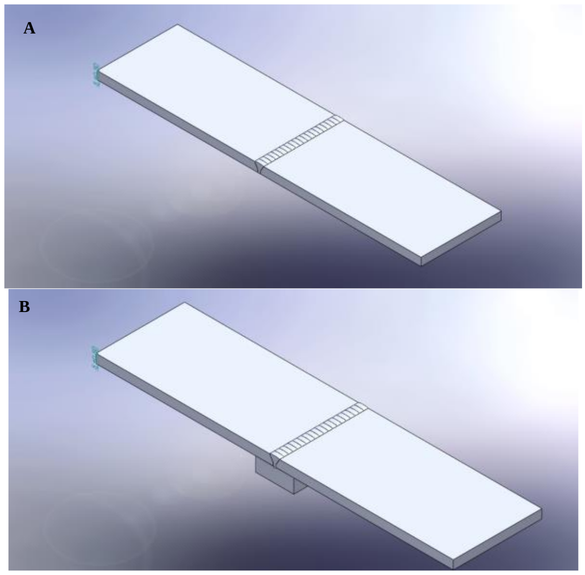

Figure 3. SOLIDWORKS models (a) without backing (b) with backing

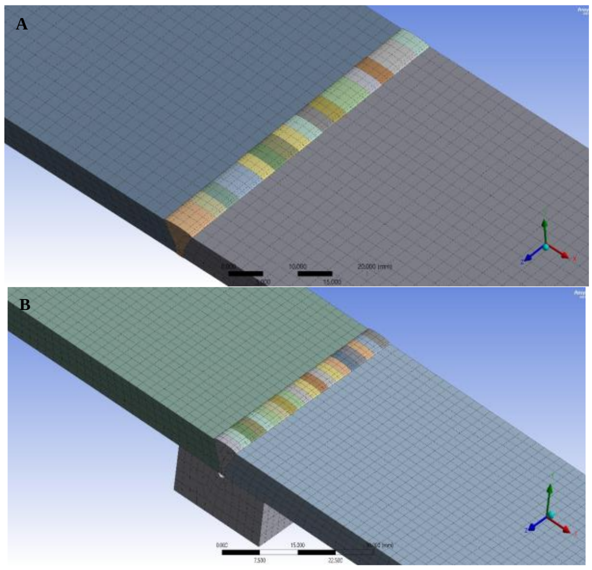

Figure 4. ANSYS models (a) without backing mesh (n) with backing mesh

Table 1. ANSYS mesh parameters of six simulation models

Without Copper Backing	Elements size	2 mm
	Elements No.	5455
	Node number	25604
With Copper Backing	Elements size	2 mm
	Elements No.	11160
	Node number	58178

Table 2. Physical and mechanical properties of AISI 304 st. st plates

Elastic Modules	193 GPa
Poisson ratio	0.275
Shear modules	74 GPa
Mass density	7930 Kg/m^3
Tensile strength	515 MPa
Yield strength	205 MPa
Thermal expansion	17.3 × 10^{-6}°C^{-1}

Consideration has been given to moving heat sources, material nonlinearity, and geometric nonlinearity. In addition, the authors used a dynamic distributed heat source model based on Goldak's double-ellipsoid heat flux distribution as an input in a finite element (FE) study of the welding process. Through it, they could anticipate variations in temperature, fusion area, heat-affected area, and contraction in both longitudinal and transverse directions, as well as any resulting alteration in angle or remaining stress. The innovative approach employs a copper backing plate to simulate and evaluate the effects of deformation and residual stress distribution in welded stainless steel. The initial phase of the research involved studying the distribution state of welding heat and its impact on deformation. Dividing a three-dimensional structural model into a finite element model It is essential to assess residual stress and deformation impacts on base metal after welding [23]. The model was meshed using ANSYS 2022 to enable a multi-physics coupling solution. The joining zone weld body was first separated into equal parts, considering the distinctiveness of the curved weld face and root; the mesh was partitioned using sweeping to achieve consistent element sizes on the weld. The resulting mesh shown in Figure 4(a) and Figure 4(b). A uniform grid can implement modified unit's "birth-death" operation to replicate creation of welds during welding. To guarantee precision of solution, mesh size for both base metal and backing plate divided into 2 mm increments. This was done since the welding in the flat plate is not the main focus of the welding deformation analysis. Given the large size of the base plate, using a small mesh size would reduce the solution's effectiveness. As a result, the mesh was split into segments of 2 mm in length. A uniform free meshing technique was used for welding zone geometry to guarantee the nodes between the components were connected, directly linking the two base plates and bottom backing plate to weld elements [24]. Moreover, in actual operational circumstances, the weldments were rendered immobile by fixtures while being welded, and these fasteners limited unrestricted expansion of base metal when heated to specific degree. During creation of finite element model, movement and rotation of bottom surface of weldment and base plate were constrained at two weldment edges.

This study was conducted in two phases. During the Initial stage, a transient thermal analysis was performed to simulate the heat distribution during welding and estimate the heat-affected zone (HAZ) dimensions and the welding fusion zone. The dynamic motion of the heat source for the two joints was analyzed using a heat-distributed model. In the second phase, the results of the transient heat analysis were used to predict residual stress and distortion for the two joints and evaluate the effects of the copper backing plate on welding using mechanical breakdown. For accurate welding process simulation and to match the actual welding condition, the welding joint was divided into equal parts when designed by SOLIDWORKS. The welding joint was 50 mm long and divided into 20 similar pieces, with 2.5 mm for each part; then, a 2000°C welding temperature was applied for the first part of the joint, starting with 1 sec. Time-temperature gradient from 2000°C part toward the rest of the 20 parts calculating for both directions, ANSYS software was used in calculating this gradient according to the deposited filler and base material boundary condition. This procedure is repeated in the second part but with 2 sec. Time, and so on; this technique will produce a moving welding point with a more realistic heat distribution with time. The results of the welding heat distribution according to the previous methods in transit thermal simulation of this steep-used in estimated the fusion zone dimension, HAZ (heat affected zone) dimension, and the welding deposited metal penetration between the passes, then the transit thermal simulation model connected to static structure model in ANSYS to calculating the deformation and the residual stress for the two welding joints.

3. THERMAL ANALYSIS AND HEAT MODELING

During the electric arc welding process, an electrical source creates a voltage differential U between the electrode and the base metal, forming an electric arc. The process entails energy dissipation from radiation and convection within the weldments and electrodes. Hence, only fraction of energy is utilized for material melting, necessitating the inclusion of power efficiency (denoted by the symbol ŋ) as a variable. Therefore, the precise representation of the weld heat input is given by the following expression:

$$Q = \eta . U . I \tag{1}$$

The thermal model used in this work applied the heat flux equation described in Eq. (2), allowing for the thermal gradient assessment within a three-dimensional object. This evaluation utilized energy balance on control volume inside designated research region. As per the study of Bezerra and Rade [25], it has been determined that the object experiences non-linear heat transfer, primarily due to the significant influence of the thermophysical properties of the materials involved, which exhibit a noticeable correlation with temperature.

$$\begin{aligned} \rho(T)c(T)\frac{\partial T}{\partial t} &= Q + \frac{\partial}{\partial x}\left[K_x(T)\frac{\partial T}{\partial X}\right] \\ &+ \frac{\partial}{\partial y}\left[K_y(T)\frac{\partial T}{\partial y}\right] + \frac{\partial}{\partial z}\left[K_z(T)\frac{\partial T}{\partial z}\right] \end{aligned} \tag{2}$$

The densities ρ, specific heats c, and heat inputs Q are given by the above equation labeled as Eq. (2). Other variables include conductivity coefficients in three directions K_x, K_y, and K_z. All these factors affect temperature T. Their change with time can also be expressed mathematically as heat loss due to convection (q_c) and radiation (q_r).

$$q_c = h_f(T - T_\infty) \tag{3}$$

$$q_r = \varepsilon\sigma(T^4 - T_\infty^4) \tag{4}$$

h_f represents the convective coefficient, while T_∞ represents the ambient temperature. The Stefan-Boltzmann constant is denoted by σ, and ε refers to the emissivity of the body's surface. During the process, if there is a phase change that occurs, also known as latent heat, it can be expressed as function of enthalpy H using following equation:

$$H = \int \rho c \, dT \tag{5}$$

The accurate depiction of the heat source is a pivotal stage in conducting Finite Element Method (FEM) Analysis. Goldak presented. This equation is derived from investigating and modeling the dispersed heat source related to arc welding. The result was the computational determination of temperature distribution. In particular, for these purposes. The boundary condition for thermal analysis in the ANSYS model is fixed as the melting temperature of stainless steel at the welding zone, which is 2000°C. By utilizing Adams equation as depicted in Eq. (6), the maximum temperature at a specific distance (Y) from the fusion line in the welding zone can be ascertained to establish the length of the heat-affected zone (HAZ) for each joint design. This distance is determined based on when the temperature falls below 723°C, as no phase transition occurs below this temperature.

$$\frac{1}{tp - to} = \frac{5.44 \, \pi k \, \alpha \, v}{Qv} \left[2 + \left(\frac{vy}{2\alpha} \right)^2 \right] + \frac{1}{tm - to} \tag{6}$$

The equation mentions that the peak temperature for a certain distance (y) is labeled as tp, and initial temperature of metal is denoted as $t0$. The welding speed is set beforehand and represented by V (mm/sec.). The term k represents the thermal conductivity of the workpiece, while Q stands for the welding heat input. The symbol α denotes the workpiece's thermal diffusivity, equal to the K over ρC (where symbol ρ means the density value of material layer and C represents specific heats). Finally, the melting temperature specified for 304 stainless steel (tm) was 1450°C.

4. MECHANICAL ANALYSIS

The temperature history of the nodes in the finite element mesh is computed and stored during the thermal analysis for the mechanical analysis. During structural analysis, temperature histories were utilized as thermal loading to generate a residual stress field. Consequently, thermal stresses and strains may compute every temporal increment [26]. Thermal elastoplastic material model relies on Von Mises yield criteria and isotropic strain hardening rule. Mechanical analysis employs the same mesh as the thermal investigations, based on the heat outcomes of the trainset. Stainless steel base metal and weld metal do not undergo solid-state phase change when welding. Hence, overall rate of deformation may state as follows:

$$\varepsilon \; total = \varepsilon_e + \varepsilon_p + \varepsilon_{th} \tag{7}$$

The equation below shows the relationship between elastic strain (ε_e), plastic strain (ε_p), and thermal strain (ε_{th}). Elastic strain is calculated using isotropic Hooke's law, incorporating temperature-dependent Young's modulus and Poisson's ratio [27]. Thermal strain calculated using temperature-dependent coefficient of thermal expansion. Plastic strain is modeled using strain-dependent plastic model that includes following features: temperature-dependent mechanical properties and a linear kinematic hardening model. Including kinematic hardening is vital because material points undergo loading and unloading during welding.

5. COUPLING THERMAL AND MECHANICAL SIMULATION PROCESS

The process of building the linked thermo-mechanical model involved making certain assumptions. The little impact of heat generated by stress deformation on temperature field disregarded due to its insignificance compared to dominant influence of the transient thermal field on mechanical characteristics. Temperature field's latent heat of phase change and stress field's weak phase transition generated by stress are disregarded. Influence of fluid movement in the melt pool due to body force is also broken. Numerical simulation employs indirect coupling, wherein the solution technique consists of two distinct phases. The initial stage involves conducting nonlinear transient thermal analysis to get dynamic thermal distribution and its progression in fusion zone and its vicinity. Subsequently, a linear static stress analysis is performed. Temperature distribution on nodes utilizes a thermal load in stress analysis and is then applied to subsequent mechanical elastic-plastic calculation. Figure 5 illustrates comprehensive process for coupling analysis diagram. Boundary conditions are employed in mechanical computation to inhibit rigid body motion. Due to the symmetrical nature of finite element (FE) model, symmetry plane rigidly set at both ends of the weldment in the thickness direction.

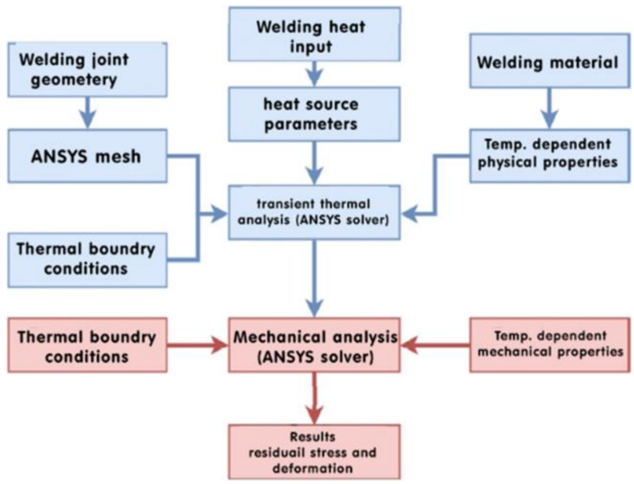

Figure 5. ANSYS coupled transient thermal and mechanical analysis procedure

6. NUMERICAL CALCULATION AND ANALYSIS

The following stages outline the results, together with a discussion on temperature prediction, residual stress, and distortion:

6.1 Analysis of welding temperature field in base metal

Temperature readings are taken at several sites and recorded every 5 seconds. Experiments were conducted to determine the calculated temperature distributions, heat-affected zone dimensions, fusion zone dimensions, and their variations over time for both models with and without backing. Figures 6 and 7 display time-dependent welding temperature cycles measured at various points inside the weldment. The results above demonstrate a clear proportionality between the fluctuations in temperature and time for all five chosen sites and both joints.

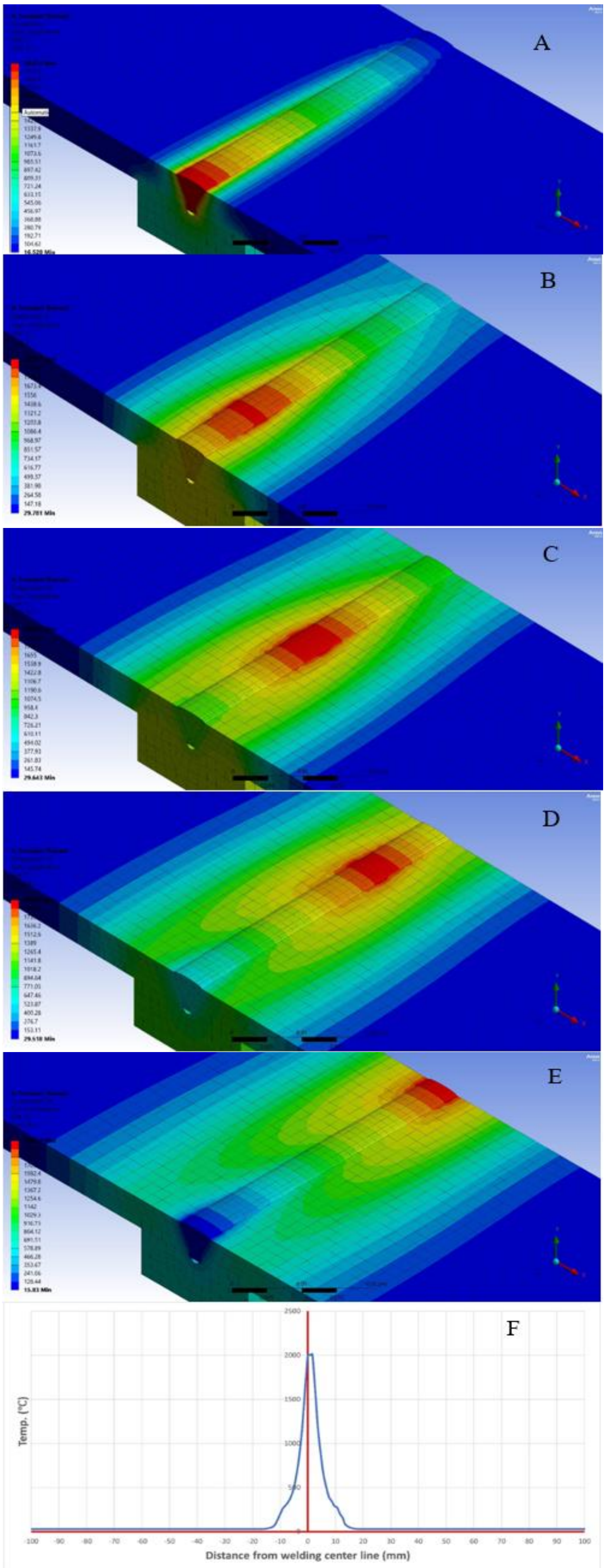

Figure 6. Joint with backing moving heat distribution according to time and distance (a) 1 sec. (b) 5 sec. (c) 10 sec. (d) 15 sec. (e) 20 sec. and (f) heat distribution from the welding center line (mm)

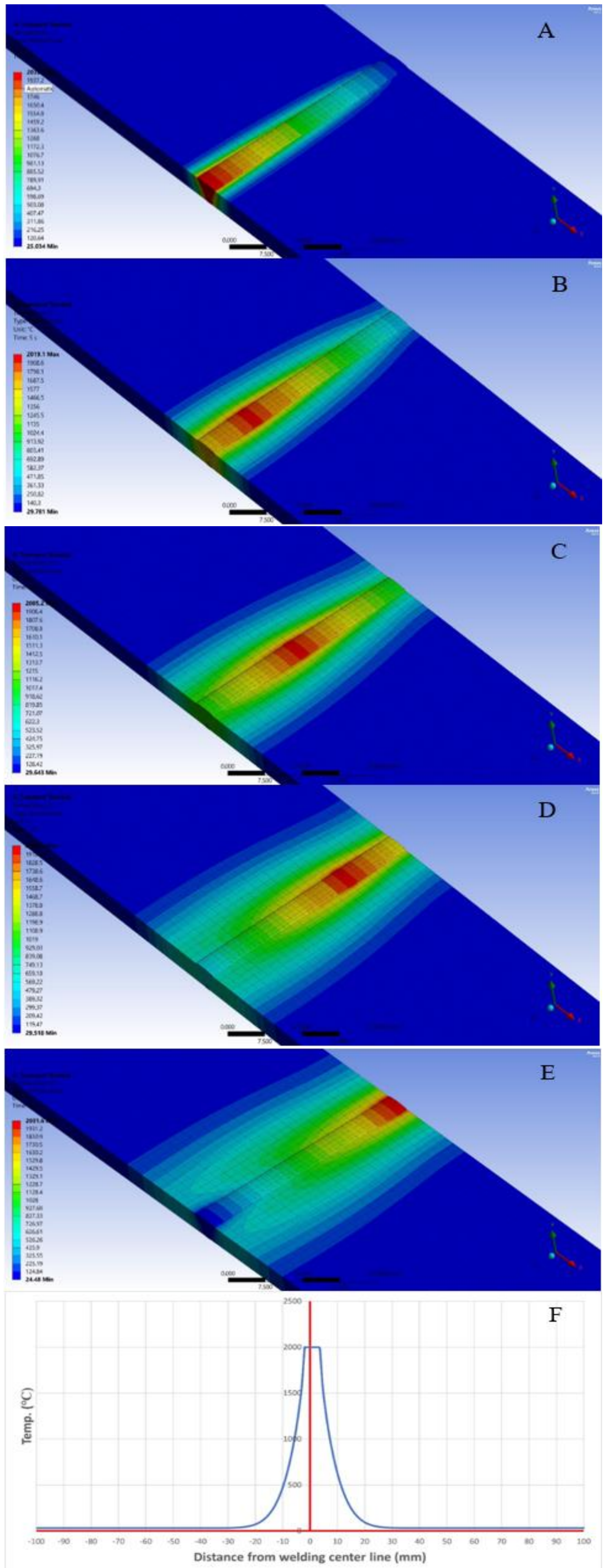

Figure 7. Joint without backing moving heat distribution according to time and distance (a) 1 sec. (b) 5 sec. (c) 10 sec. (d) 15 sec. (e) 20 sec. and (f) heat distribution from the welding center line (mm)

The heat distribution in Figure 6 shows high heat distraction toward the copper backing plate, which can be noticed from the change in copper plate color according to the heat flow and the differences in far edge temperature estimated by the simulation in 1 and 20 sec. The two models (with and without backing) display strong evidence about the copper plate effects in welding heat distraction; for welding with a backing plate, the temperature of the edge in welding starts after 1 sec. In welding end after 20 sec., as shown in Figures 6(a) and (e), was 16.5℃ and 15.8℃, while the edge temperature was 25℃ and 24.48℃ for 1 sec. And 20 sec. Respectively for the simulation model without backing in Figures 7(a) and (e). The heat distribution diagram for the welding model with a backing plate in Figure 6(f) demonstrated a narrower peak temperature in the fusion zone and a sharper dropping slope from the peak welding temperature to the room temperature than the heat distribution diagram in Figure 7(f) which illustrated the copper plate impacts on welding temperature distribution. The heat-affected zone (HAZ) is critical in stainless steel weldments; the temperature range between 1200℃ to 723℃ will determine the (HAZ) dimension.

Grain growth reaction was one of the significant changes during a high-intensity 1200℃ thermal cycle. Since the grain boundary movement at this exact temperature is more important than any other heating cycle, it follows naturally when transitioning from one peak to another. Moreover, new grains are created. It's been discovered that austenitic steels that are welded or subjected to high temperatures for extended periods usually lose their glassy state ceasingly over time [28]. Cyclic temperature changes cause carbon to precipitate as carbides at temperatures of 800℃ and 900℃. Mn_5C_2, Mn_7C_3, and $Mn_{23}C_6$ carbides are the main carbides observed in 304 stainless steel [29]. For physical properties such as hardness and toughness studies, these carbides often increase the hardness in HAZ, but hardness drops over 90℃. It is due to grain growing and carbides dissolving. Even more critical, Kozuh et al. propose that there are still reductions in the stresses and changes in microstructure involved [30, 31]. The formation and dissolving of these metallic compounds are intensely engaged in mechanical properties and austenitic stainless steel microstructure, which is constantly being processed by machine work, welding, and heat treatment. The formation of this problem was connected in fully austenitic metals to be intrinsic to the presence of coarse grains (formed by recrystallization and grain growth), which caused an elevated risk for liquation cracking; all these phenomena are dependent on welding temperature distribution and HAZ width [31].

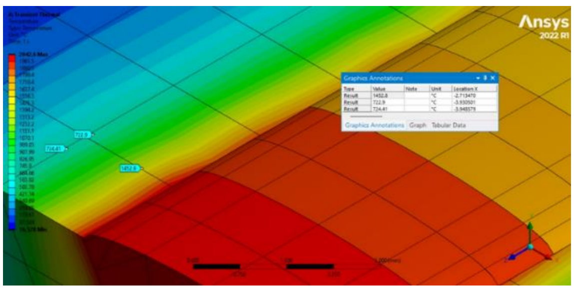

(a) 1 sec

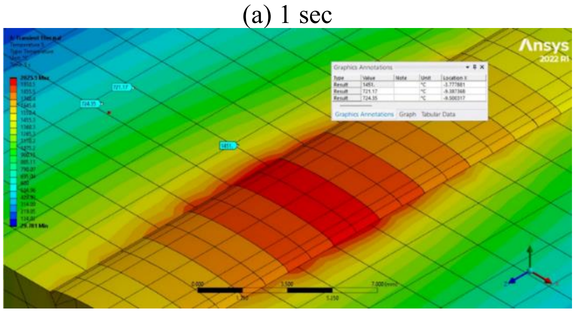

(b) 5 sec

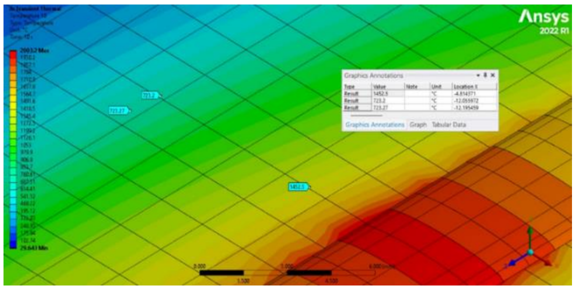

(c) 10 sec

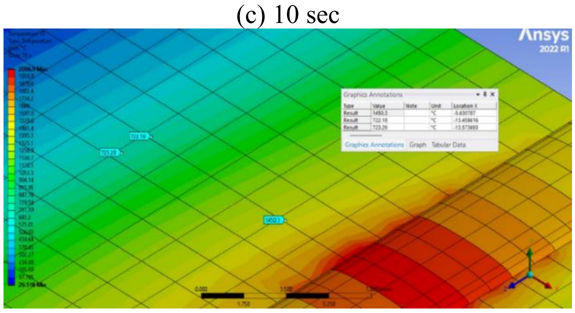

(d) 15 sec

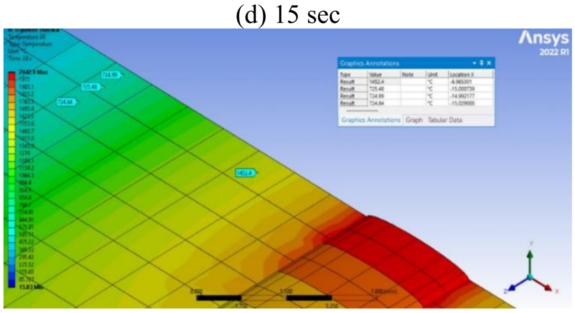

(e) 20 sec

Figure 8. Joint without backing moving heat HAZ and FZ

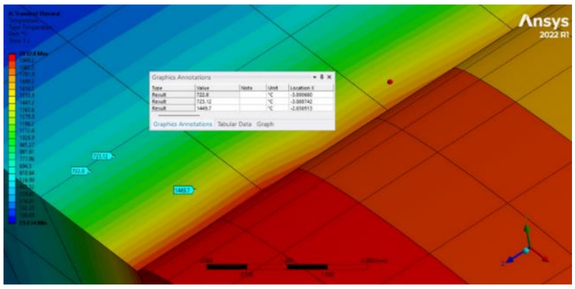

(a) 1 sec

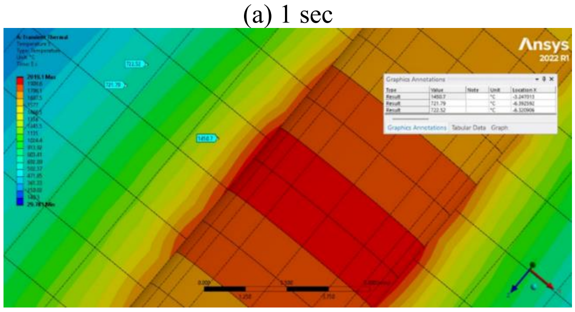

(b) 5 sec

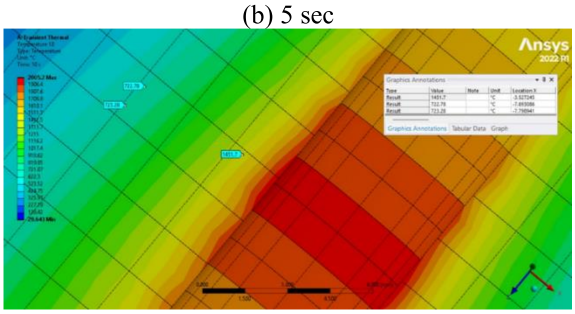

(c) 10 sec

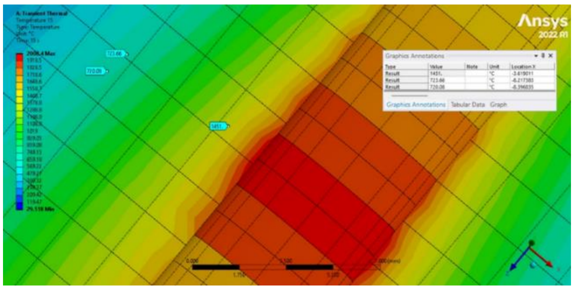

(d) 15 sec

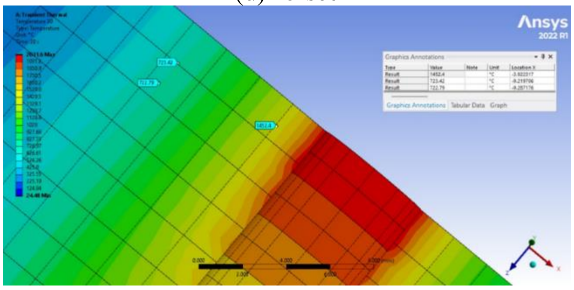

(e) 20 sec

Figure 9. Joint with backing moving heat HAZ and FZ

Table 3. Without backing and with backing joints, HAZ width with welding time progress

Time (sec.)	Without Backing	With Backing
1 sec.	3.9	3.8
5 sec.	9.5	6.3
10 sec.	12.1	7.7
15 sec.	13.5	8.3
20 sec.	15	9.2

The calculation of the HAZ and fusion zone boundaries using ANSYS 2022R1 is presented in Figures 8 and 9 for two models, one with backing and one without, across five different times (1, 5, 10, 15, and 20 seconds).

The simulation models depicted in Figures 8 and 9 show the minimum dimension of the HAZ at the start of welding at 1 second. As time progresses during welding, the HAZ width increases, with the maximum width observable at the welding end at 20 seconds. This expansion is due to the accumulation of welding heat over time. Similarly, for both models—with and without backing—the minimum dimension of the fusion zone (FZ) is estimated at the start of welding at 1 second. The fusion zone then expands to its widest at the welding end at 20 seconds.

Figure 8 illustrates the width of the heat-affected zone (HAZ) for a weldment joint without backing, starting from 3.9 mm with a 1-second duration as shown in Figure 8(a), and reaching a maximum HAZ width of 15 mm at the welding end after 20 seconds as shown in Figure 8(e). Conversely, Figure 9(a) demonstrates the HAZ width for a weldment joint with a copper backing plate, also for a 1-second duration; the simulation result shows a HAZ width of 3.8 mm, which is almost identical to that of the weldment without backing. However, the remaining results show significant differences for durations of 5, 10, 15, and 20 seconds between the two models, as detailed in Table 3. Figure 9(e) indicates a maximum HAZ width of 9.2 mm after 20 seconds at the welding end, which is 38.67% less than the corresponding result for the welding joint without backing. These results confirm the effectiveness of the copper backing plate in reducing the impact of welding heat on the HAZ width and heat distribution in stainless steel weldments. Due to its excellent thermal conductivity properties, the copper backing plate rapidly absorbs heat from the weld pool. Consequently, the heating at high temperatures is reduced in the heat-affected zone, leading to lesser alterations in metallurgical transformations and mechanical properties.

6.2 Analysis of welding deformation

Reduction of deformation is a critical function of the backing plate in stainless steel welding. The heat produced by welding alters the material structure by causing recrystallization, grain growth, and precipitate dissolution, a well-known phenomenon. It should be noted that because of specific characteristics, austenitic stainless steels are especially vulnerable to distortion when welding. When we weld, the material may bend or shift, which is distortion. Due to its compromise of strength and functionality, this distortion can present problems for welded structures.

The experimental results show that the angular distortion is reduced using a groove angle that is 60º V-shaped. For steel plates, the outcomes were also comparable [32]. Figure 5 displays the result of an additional study [33]. Because of the variation in transverse shrinkage throughout the specimen's thickness, angular distortion in single V-groove butt weldments decreased as included angle raised. Mechanical analysis utilizes the large displacement hypothesis to examine distortions caused by welding. This study employs dynamic thermal source profiles to evaluate the deformation occurring in the x (transverse) direction under specific boundary conditions. The results from the ANSYS simulation models, depicted in Figures 10 and 11 for weldments without and with backing plates, respectively, demonstrate significant differences. The maximum deformation in the weldment without backing plates, found at the weld joint's end, is 1.17 mm, representing 23.4% of the weldment thickness, as shown in Figure 10(a). In contrast, the deflection at the same location for the weldment with a backing plate is 0.82 mm, approximately 16.4% of the weldment thickness, as depicted in Figure 11.

Furthermore, the maximum deformation in the weldment with backing occurs at the corner of the copper backing plate, far from the welding joint, measuring 0.97 mm, as illustrated in Figure 11(b). This occurs due to the heat absorption by the copper backing plate and its dissipation to the outer environment. The notable difference in deflection values between the two models, approximately 7%, reflects the effectiveness of the copper backing in reducing deformation at the welding joint and ensuring the joint dimensions meet design requirements.

The location of maximum deformation in the welding zones for both models, as illustrated in Figures 10(b) and 11(c), results from prolonged exposure of these zones to high temperatures during welding. This prolonged exposure alters the zone's properties, changing as a function of temperature, which affects both mechanical and thermal characteristics [34]. At approximately 800°C, the latent heat enhances the specific heat and other properties associated with phase transitions. The thermal expansion ratio (TER) indicates that this comparison is the ultimate consequence of the phase transition. Beyond temperatures of 600-700°C, the yield stress becomes negligible. At this point, the material's flexibility and ease of deformation increase significantly, as the yield stress is almost nonexistent. Around these temperatures, the material behaves more like a liquid and loses its resistance to deformation, a phenomenon referred to as the mechanical melting point.

Furthermore, the findings demonstrate that the positioning of the fixtures is crucial in defining the deformation effect zone. By securing the two welding edges and allowing the welding joint to move freely, the maximum distortion zone in this study was directed towards the joining center line.

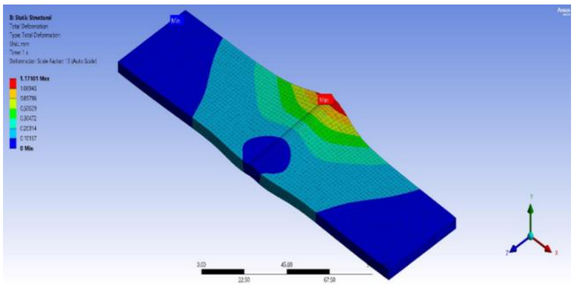

(a) maximum deformation location

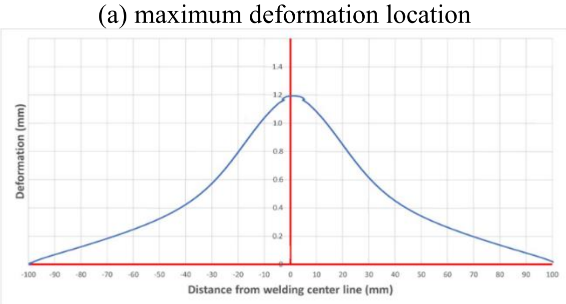

(b) deformation distribution along the weldment X-axis

Figure 10. Joint without backing deformation

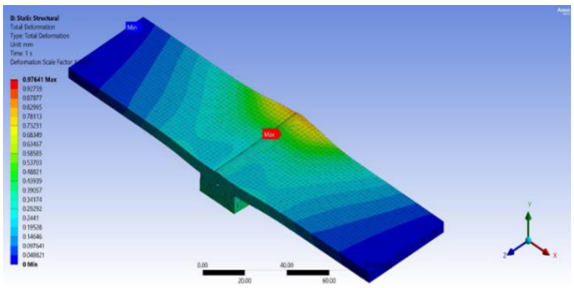

(A) maximum deformation location

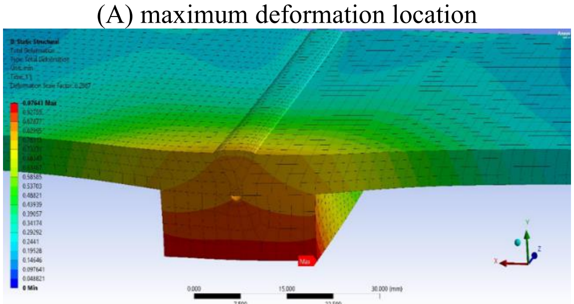

(B) backing plate maximum deformation

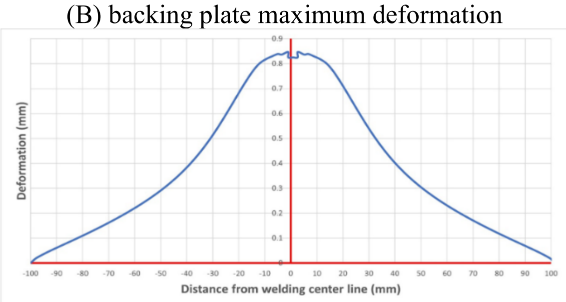

(C) deformation distribution along the weldment X-axis

Figure 11. Joint with backing deformation

6.3 Analysis of welding residual stresses

Welding residual stresses at top and bottom surfaces of welding plate with no backing plate and with the backing plate are carried out from the fully constraint edges of the weldment to the welding center line for both sides. Figures 12 and 13 illustrate the strained cases for models with and without a backing plate. For both models, the peak value of longitudinal stress occurs at the x-axis at the top surface of the welding joint line end. However, the locations of these peak stresses differ between the two models, as evident from the residual stress distribution diagrams shown in Figures 12(b) and 13(b). These diagrams indicate that the stress is higher at the top surface than at the bottom surface of the welding joint. Figure 12(a) shows the location of maximum stress for the model with a backing plate, with the highest stress found at the welding fusion boundary on the top surface of the joint zone in the welding center. In contrast, Figure 13(a) illustrates the locations of maximum stresses for the model without a backing plate, with the highest stress observed at the upper top of the joint face.

Welding involves applying a great deal of heat to a small joint area. This area and those around it are molten, allowing the joint's parts to fuse. The dispersion of heat inside the joint is both irregular and dynamic. As mentioned before, the joint experiences thermal expansion of varying magnitudes because of the uneven distribution of temperatures. To compensate for the joint's variation, stresses and distortion are caused by elastic and plastic strains. One possible interpretation of the temperature field is that it is highly concentrated around the heat source and relatively low in the surrounding area due to the severe temperature gradient. Of course, the surrounding region will act as a brake on the high-temperature zone's thermal expansion. Under the quasistatic situation, the same temperature field is moving in a long butt joint, as mentioned before. Due to this circumstance, the joint's transverse section is expected to remain flat during welding throughout most joints, except the beginning and finish. According to that, the molten welding metal at the welding fusion line will be the first solidified metal due to the high cooling rate of this zone because it is adjacent to the cold base metal and would test high thermal stress due to the high temperature of the molten metal. The magnitude of these stresses will depend on two main factors: the temperature difference between the molten metal and the cold base metal. Second, how fast can this difference be reduced, or, in other words, how quickly can the metal get rid of welding heat, which produces thermal stresses when welding with copper backing? The copper works as a heat sink and wastes the welding heat with a speedy cooling rate from the joint; this will reduce the residual stress and welding joint deformation. For this reason, the maximum stress value in weldment with backing in Figure 12 is lower than that in Figure 13 for weldment without value because there is no welding heat distraction. The maximum stress location in Figure 12(a) resulted from the prolonged cooling rate of the welding fusion line at the weldment center due to the continuous exposure to welding heat from the welding starting point to the weld center and from this point to the welding end, which produced the maximum stress in this point. The rest of the welding joint will test a faster cooling rate due to the copper plate effects and the shorter temperature exposure time. Figure 13(a) shows different maximum stress locations at the top of the welding bead surface end due to cumulative welding temperature at this point from the welding starting to the welding end. In addition, exposure to the melting temperature at the last welding second without any outer heat distraction and relatively poor stainless steel heat conductivity resulted in high deformation at this point.

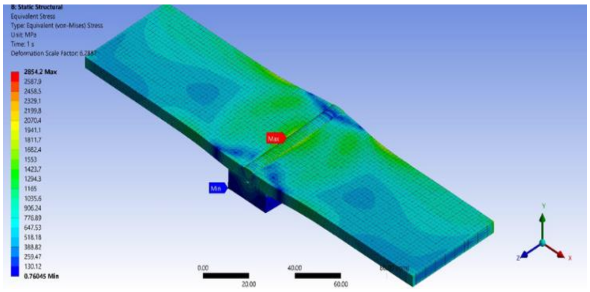

(a) Max. and Min. stress location

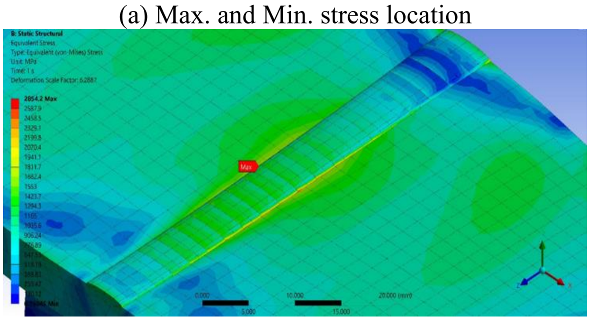

(b) Maximum stress

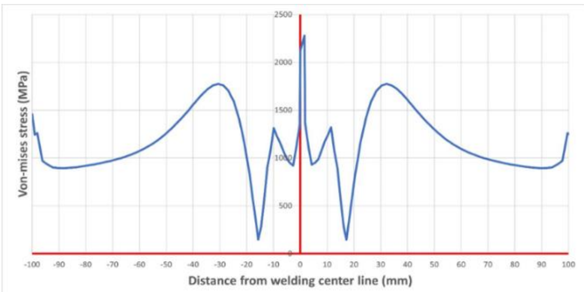

(c) Stress distribution along the weldment X-axis

Figure 12. Joint with backing stress

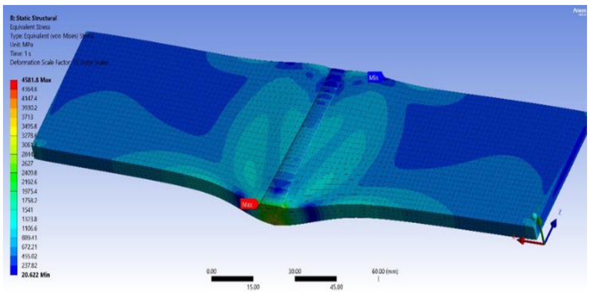

(a) Max. and Min. stress location

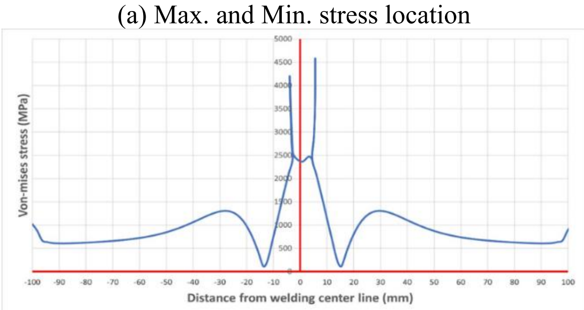

(b) Stress distribution along the weldment X-axis

Figure 13. Joint without backing stress

7. EXPERIMENTAL VALIDATION OF THE SIMULATION MODEL

This study examined the effects of a backing plate on the deformation, microstructure, and mechanical characteristics of the welding zone. Two different welding procedures were employed: one with a backing plate and one without, as illustrated in Figures 14(a) and (b). There was a negligible discrepancy between the simulation and experimental deformation values of the two welding samples. For example, although the ANSYS model predicted a maximum deformation value of 0.82 mm for the welding joint with a backing plate, the actual measurement reached 0.90 mm. Similarly, the experimental deformation for the sample without backing was 1.17 mm, approximately 23% of the sample thickness; the exact measurement came out to 1.21 mm. The authors clarify that this little discrepancy results from the virtual environment's cooling rate differing from the one used in the ANSYS model solution technique.

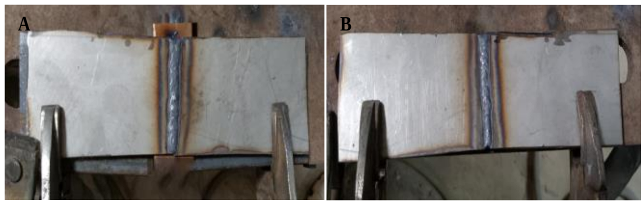

Figure 14. (a) Joint with copper backing, (b) Joint without copper backing

Lathy δ ferrite

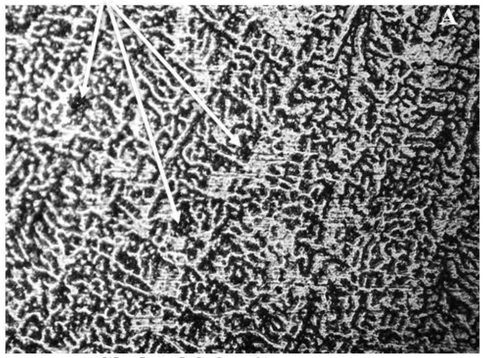

Skeletal δ ferrite

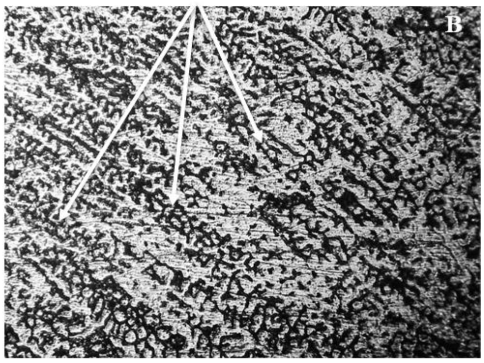

Figure 15. (a) Weld zone without copper backing microstructure, (b) weld zone with copper backing microstructure backing

Both welded joints exhibit austenite (γ) and ferrite (δ) following the whole solidification process at room temperature, as seen in the optical micrographs in Figure 15(a) and (b). Two forms of ferrites (δ), skeletal δ-ferrite and lathy are generated in an austenitic matrix in the fusion zone. The weld metal sample without backing, shown in Figure 15(a), exhibits a high concentration of lathy δ-ferrite in the microstructure of the welding zone. In contrast, the sample with a backing plate, displayed in Figure 15(b), reveals a more substantial concentration of skeletal δ-ferrite. The welding process causes the austenite growth to reject Cr from the structure, and the absorption of Ni causes a high concentration of Cr and depletion of Ni in residual ferrite [35]. Usually, the transformation from ferrite to austenite in stainless steel is a gradual process controlled by diffusion of elements. However, this transformation is incomplete during welding due to the speedy cooling rate compounded with the welding. Stainless steel welding does not fully transition ferrite to austenite due to element diffusion impacted by the cooling process. The final microstructure of the weld metal is a skeletal δ-ferrite that stays in the dendrite cores, as seen in Figure 15. This is because the thinner lamellae ferrite solidified into austenite during the cooling process. However, the thicker primary dendritic ferrite could not dissolve entirely and remained in the dendrite cores as skeletal δ ferrite.

The cooling rate during welding is a critical factor in determining the transformation of ferrite, influenced by other elements such as the amount of heat generated in the welding molten pool, the thermal gradient, and the heat dissipation through the base plate. Both Figure 15(a) and Figure 15(b) illustrate different types of ferrite transformations. The weld metal microstructure shown in Figure 15(b) displays the most significant heat extraction and temperature gradient through the base metal, indicating the highest level of supercooling. As a result, the stabilizing austinite elements will not be able to diffuse adequately over the ferrite, leading to the austenite transformation. The end outcome of the transformation process is the production of lathy δ ferrite and δ ferrite skeletal morphology type but with high skeletal δ ferrite concentration [36]. This result proved the effects of backing plate on thermal distribution and gradient in welding zone and HAZ. This study focused on the impacts of the copper backing plate in minimizing the distortion of the stainless steel weldments without testing the effects of changing the packing plate materials or welding with different fusion welding technologies; this limitation could be a good research direction for future work.

8. CONCLUSIONS

The effects of a copper backing plate on heat distribution, residual stress, deformation, and stainless steel welding have been investigated in this research using the ANSYS simulation software. Weld deformation in this study showed that using a copper backing plate drastically decreased weld deformation. The weldment with a backing plate had more minor maximum deformation than without. The stability offered by the backing plate mitigates distortion and preserves the weld joint's integrity, which in turn reduces deformation.

The results show that using a backing plate helps reduce welding distortion in stainless steel weld connections from 23.4% to 16.4% of the thickness. Weldment residual stress in this investigation showed that a copper backing plate decreased weldment residual stress. When comparing the two types of weldments, the one with a backing plate had lower maximum stress values. Because copper is a good heat conductor, it aids in dissipating welding heat and reducing temperature gradients in the weld, which contributes to decreasing residual stresses. Maximum residual stress in the simulation model with a backing plate was recorded at the fusion line in the weldment center. It was less by 62.2% than the maximum residual stress value of the simulation model without backing, which was recorded at the welding bead top surface. It proved the impacts of the copper backing plate during welding reduced thermal strains and temperature gradients since it absorbs and dissipates the heat.

A smaller fusion zone peak temperature and a steeper decreasing slope from the peak welding temperature to room temperature were seen in the examination of the welding temperature field when a copper backing plate was present. Simulation results illustrated a maximum HAZ width of 9.28 mm when welding with a backing plate and 15 mm when welding without backing. This proves that the backing plate regulates heat dispersion and reduces the HAZ size. Using a backing plate efficiently reduces the heat impacts of welding, as shown by the simulation findings, which also showed that the HAZ width and fusion zone width were decreased. The weld zone microstructure examination proved the defects in heat distribution in the welding zone and the alteration in cooling rate due to the backing plate effects, which the ANSYS model calculated.

The long-term effect of applying the copper essential plates is the increasing possibility of galvanic corrosion between the copper and the stainless steel. Copper is a very autorotative metal into which stainless steel can be plated. This may create an electrochemical cell between the copper and the stainless steel, wherein the copper acts as an anode while the stainless steel is the cathode. The process may cause a lot of corrosion in the surrounding stainless steel when the copper plate is used as the backing. To conclude, the crucial role of copper backing plates in stainless steel welding joints is that the steel joints are very effective only if there is good copper at all the points where each of the two parts of the joint are joined. Furthermore, the welded joint must be very well-designed and maintained. A primary objective is to identify the possible implications for the many industries involved in a particular application of the joint assembly. Venture into the operating conditions will largely determine how successfully the welded joint will function. For example, in the food and pharma industries, where hygiene and corrosion resistance are essential, regulation or additional precautions should be taken to ensure the longevity of the welded joints with copper backing plate.

REFERENCES

[1] Li, Z., Feng, G., Deng, D., Luo, Y. (2021). Investigating welding distortion of thin-plate stiffened panel steel structures by means of thermal elastic plastic finite element method. Journal of Materials Engineering and Performance, 30: 3677-3690. https://doi.org/10.1007/s11665-021-05646-y

[2] Abdulameer, A.G., Mohammed, M.S., Abbas, A.S. (2022). Microstructure variation effects influence on characteristics and mechanical properties of Monel 400 and low alloy steel (ASTM 387-Gr. 11) GTAW dissimilar joint. Eastern-European Journal of Enterprise Technologies, 119(12): 13-20. https://doi.org/10.15587/1729-4061.2022.266264

[3] Wang, L., Miao, Y., Hu, G., Zhao, Y., Deng, Q. (2023).

Numerical simulations and experimental verification of T-structure welding deformation using the step-by-step loading inherent strain method. Metals, 13(7): 1312. https://doi.org/10.3390/met130713124
[4] Liu, J.C., Luo, G.E., Zhang, S., Jing, S.H. (2022). Study on welding residual stress redistribution of AH36 marine high strength steel considering the crack propagation. Proceedings of the SPIE, 12309: 123091M. https://doi.org/10.1117/12.2645612
[5] Kalita, K., Burande, D., Ghadai, R.K., Chakraborty, S. (2023). Finite element modelling, predictive modelling and optimization of metal inert gas, tungsten inert gas and friction stir welding processes: A comprehensive review. Archives of Computational Methods in Engineering, 30: 271-299. https://doi.org/10.1007/s11831-022-09797-6
[6] Romero-Hdz, J., Saha, B., Toledo-Ramirez, G., Beltran-Bqz, D. (2016). Welding sequence optimization using artificial intelligence techniques: An overview. International Journal of Computer Science and Engineering, 3(11): 90-95.
[7] Mohamed, M.S., Abtan, A.A., Moosa, A.U. (2023). Microstructure and mechanical properties assessments of 304 austenitic stainless steel and Monel 400 dissimilar GTAW weldment. Journal of Composite & Advanced Materials/Revue des Composites et des Matériaux Avancés, 33(3): 135-144. https://doi.org/10.18280/rcma.330301
[8] Derakhshan, E.D., Yazdian, N., Craft, B., Smith, S., Kovacevic, R. (2018). Numerical simulation and experimental validation of residual stress and welding distortion induced by laser-based welding processes of thin structural steel plates in butt joint configuration. Optics & Laser Technology, 104: 170-182. https://doi.org/10.1016/j.optlastec.2018.02.026
[9] Djeloud, H., Moussaoui, M., Kouider, R., Al-Kassir, A., Carrasco-Amador, J.P. (2023). Study of the heat exchange and relaxation conditions of residual stresses due to welding of austenitic stainless steel. Energies, 16(7): 3176. https://doi.org/10.3390/en16073176
[10] Cordeiro, F.D.S. (2015). A critical analysis on welds distortion. Master's thesis, Universidade de Coimbra (Portugal).
[11] Venkatkumar, D., Ravindran, D. (2019). Effect of boundary conditions on residual stresses and distortion in 316 stainless steel butt welded plate. High Temperature Materials and Processes, 38(2019): 827-836. https://doi.org/10.1515/htmp-2019-0048
[12] Gunasekaran, K., Solomon, I., Skvireckas, R., Dunduliso, G. (2023). Influence of temperature variance on the mechanical properties of a welded bearing support flange under transient conditions using finite element approach. Mechanika, 29(3): 188-193. https://doi.org/10.5755/j02.mech.31209
[13] Okano, S., Mochizuki, M. (2017). Transient distortion behavior during TIG welding of thin steel plate. Journal of Materials Processing Technology, 241: 103-111. https://doi.org/10.1016/j.jmatprotec.2016.11.006
[14] Suman, S., Biswas, P. (2020). Comparative study on SAW welding induced distortion and residual stresses of CSEF steel considering solid state phase transformation and preheating. Journal of Manufacturing Processes, 51: 19-30. https://doi.org/10.1016/j.jmapro.2020.01.012
[15] Zubairuddin, M., Albert, S.K., Vasudevan, M., Mahadevan, S., Chaudhari, V., Suri, V.K. (2017). Numerical simulation of multi-pass GTA welding of grade 91 steel. Journal of Manufacturing Processes, 27: 87-97. https://doi.org/10.1016/j.jmapro.2017.04.031
[16] Duranton, P., Devaux, J., Robin, V., Gilles, P., Bergheau, J.M. (2004). 3D modelling of multipass welding of a 316L stainless steel pipe. Journal of Materials Processing Technology, 153: 457-463. https://doi.org/10.1016/j.jmatprotec.2004.04.128
[17] Stamenković, D., Vasović, I. (2009). Finite element analysis of residual stress in butt welding two similar plates. Scientific Technical Review, 59(1): 57-60.
[18] Murugan, S., Rai, S.K., Kumar, P.V., Jayakumar, T., Raj, B. (2001). Temperature distribution and residual stresses due to multipass welding in type 304 stainless steel and low carbon steel weld pads. International Journal of Pressure Vessels and Piping, 78(4): 307-317. https://doi.org/10.1016/S0308-0161(01)00047-3
[19] Zhu, X.K., Chao, Y.J. (2004). Numerical simulation of transient temperature and residual stresses in friction stir welding of 304L stainless steel. Journal of Materials Processing Technology, 146(2): 263-272. https://doi.org/10.1016/j.jmatprotec.2003.10.025
[20] Prasad, N.S., Sankaranarayanan, T.K. (1996). Estimation of residual stresses in weldments using adaptive grids. Computers & Structures, 60(6): 1037-1045. https://doi.org/10.1016/0045-7949(96)00006-5
[21] Mollicone, P., Camilleri, D., Gray, T.G., Comlekci, T. (2006). Simple thermo-elastic–plastic models for welding distortion simulation. Journal of Materials Processing Technology, 176(1-3): 77-86. https://doi.org/10.1016/j.jmatprotec.2006.02.022
[22] Cho, J.R., Lee, B.Y., Moon, Y.H., Van Tyne, C.J. (2004). Investigation of residual stress and post weld heat treatment of multi-pass welds by finite element method and experiments. Journal of Materials Processing Technology, 155: 1690-1695. https://doi.org/10.1016/j.jmatprotec.2004.04.325
[23] Zhao, W., Jiang, W., Zhang, H., Han, B., Jin, H., Gao, Q. (2021). 3D finite element analysis and optimization of welding residual stress in the girth joints of X80 steel pipeline. Journal of Manufacturing Processes, 66: 166-178. https://doi.org/10.1016/j.jmapro.2021.04.009
[24] Ordieres, J., Rodríguez, E., Bayón, A., Caixas, J., Barbensi, A., Martín, C. (2021). Determination of the influence of clamping on welding distortion applied to PS2 mock-up using finite element simulations. Fusion Engineering and Design, 166: 112327. https://doi.org/10.1016/j.fusengdes.2021.112327
[25] Bezerra, A.C., Rade, D.A. (2004). Análise térmica do processo de soldagem tig via elementos finitos. Simpósio do Programa de Pós Graduação em Engenharia Mecânica-Faculdade de Engenharia Mecânica, Universidade Federal de Uberlândia, Uberlândia-MG.
[26] Qureshi, M.E. (2008). Analysis of residual stresses and distortions in circumferentially welded thin-walled cylinders. Doctoral dissertation, National University of Sciences and Technology.
[27] Eren, İ., Karasu Asnaz, M.S. (2022). Finite element simulation and experimental validation of welding distortion of fillet welded T-joints. Politeknik Dergisi, 25(1): 455-466. https://doi.org/10.2339/politeknik.881438
[28] Minami, Y., Kimura, H., Ihara, Y. (1986).

Microstructural changes in austenitic stainless steels during long-term aging. Materials Science and Technology, 2(8): 795-806. https://doi.org/10.1179/mst.1986.2.8.795

[29] Maistro, G. (2018). Low-temperature carburizing/nitriding of austenitic stainless steels: Influence of alloy composition on microstructure and properties. Doctoral dissertation, Chalmers University of Technology.

[30] Guo, Y.H., Lin, L., Zhang, D.H., Liu, L.L., Lei, M.K. (2018). Microstructure and mechanical properties of heat-affected zone of repeated welding AISI 304N austenitic stainless steel by Gleeble simulator. Metals, 8(10): 773. https://doi.org/10.3390/met8100773

[31] Kujanp, V., Suutala, N., Takalo, T.K., Moisio, T.J.I. (1980). Solidification cracking-estimation of the susceptibility of austenitic and austenitic-ferritic stainless steel welds. Stainless Steel, 12(6): 282-285.

[32] Bachorski, A., Painter, M.J., Smailes, A.J., Wahab, M.A. (1999). Finite-element prediction of distortion during gas metal arc welding using the shrinkage volume approach. Journal of Materials Processing Technology, 92: 405-409. https://doi.org/10.1016/S0924-0136(99)00161-2

[33] Pathak, D., Singh, R.P., Gaur, S., Balu, V. (2021). Influence of groove angle on hardness and reinforcement height of shielded metal arc welded joints for low carbon AISI 1016 steel plates. Materials Today: Proceedings, 38: 40-43. https://doi.org/10.1016/j.matpr.2020.05.597

[34] Ueda, Y., Fukuda, K., Tanigawa, M. (1979). New measuring method of 3-dimensional residual stresses based on theory of inherent strain. Journal of the Society of Naval Architects of Japan, 1979(145): 203-211. https://doi.org/10.2534/jjasnaoe1968.1979.203

[35] Leone, G.L., Kerr, H.W. (1982). The ferrite to austenite transformation in stainless steels. Welding Journal, 61(1): 13S-21S.

[36] Lippold, J.C., Kotecki, D.J. (2005). Welding Metallurgy and Weldability of Stainless Steels. Handbook of Adhesion, 2nd Edition.